Absence of thermalization of free systems coupled to gapped interacting reservoirs

Marko Ljubotina,[1,2] Dibyendu Roy,[3] and Tomaž Prosen[1]
[1]*Physics Department, Faculty of Mathematics and Physics, University of Ljubljana, 1000 Ljubljana, Slovenia*
[2]*IST Austria, Am Campus 1, 3400 Klosterneuburg, Austria*
[3]*Raman Research Institute, Bangalore 560080, India*

(Received 30 June 2021; revised 25 July 2022; accepted 19 August 2022; published 31 August 2022)

We study the thermalization of a small XX chain coupled to long, gapped XXZ leads at either side by observing the relaxation dynamics of the whole system. Using extensive tensor network simulations, we show that such systems, although not integrable, appear to show either extremely slow thermalization or even lack thereof since the two cannot be distinguished within the accuracy of our numerics. We show that the persistent oscillations observed in the spin current in the middle of the XX chain are related to eigenstates of the entire system located within the gap of the boundary chains. We find from exact diagonalization that some of these states remain strictly localized within the XX chain and do not hybridize with the rest of the system. The frequencies of the persistent oscillations determined by numerical simulations of dynamics match the energy differences between these states exactly. This has important implications for open systems, where the strongly interacting leads are often assumed to thermalize the central system. Our results suggest that, if we employ gapped systems for the leads, this assumption does not hold.

DOI: 10.1103/PhysRevB.106.054314

I. INTRODUCTION

Microscopic analysis of quantum transport, especially nonequilibrium transport across a system, is often carried out by connecting the boundaries of the system to two or more reservoirs [1–3]. These reservoirs act as a source or sink of conserved quantities, e.g., charge, energy, and spin. They are generally maintained at a fixed bias by keeping them, e.g., at different chemical potentials or temperatures or magnetizations. The explicit inclusion of such an interface between a system and a reservoir is essential in understanding the role of decoherence and dissipation (induced by the reservoir to the system) in controlling the quantum transport in physical systems [4–8]. For example, the difference between the Landauer's four-probe and two-probe resistance arises from the contact resistance due to such interfaces [4,5,9]. Apart from acting as a perfect source or sink, a reservoir should also thermalize the system to which it is connected. Therefore, it is crucial to investigate the essential properties of a reservoir to implement the above-prescribed tasks.

In most theoretical studies, the reservoirs are traditionally modeled as large (infinite) collections of harmonic oscillators or noninteracting electrons or spins [7,10–15]. The large-reservoir-volume limit is taken to ensure very long (practically infinite) Poincaré recurrence time so that the particle, or any local packet of a conserved quantity, once transferred to the reservoir is not fed back to the system. Nevertheless, these noninteracting models of reservoirs neither thermalize themselves in strict quantum mechanical sense nor do they provide any mechanism for mixing or relaxation for the transported degrees of freedom entering from the system. One then assumes some thermal statistical ensemble for these reservoirs from the outset. However, the absence of mixing in the noninteracting reservoirs creates further issues when their energy dispersion does not cover all the system's energy levels. For example, it has already been demonstrated that a system is not thermalized by such noninteracting reservoirs when one or more energy levels (bound states) of it lie either outside the reservoir's energy band or inside the energy gap of the reservoir spectrum [16–19]. These bound states are mostly localized within the central system's Hilbert space and do not leak out in the reservoir. One can simply consider the hybrid system as a conductor sandwiched between insulators, and the energy transport through the boundary reservoirs (insulators) is blocked leaving the conductor in a nonthermal state. Notably, there is no unique long-time steady-state for such a coupled system-reservoir in the presence of bound states, and transport properties across the system depend on the initialization of the full system.

It is thus intriguing to examine if the inclusion of interactions between the reservoir's degrees of freedom can help in thermalizing the system with the reservoir in the presence of bound states, i.e., the central system eigenenergies gapped away from the spectrum of the infinite reservoirs. Such an energy gap in the spectrum of a reservoir with nontrivial interactions between its constituents can naturally occur in many physical setups where the reservoirs are superconductors, correlated magnets, or other strongly correlated materials. One would naively expect that system-reservoir interactions would mix the bound states and eventually thermalize the system with the reservoir. Nevertheless, it is a nontrivial problem to analytically study such a coupled system-reservoir as the dynamical evolution of inhomogeneous interacting systems is

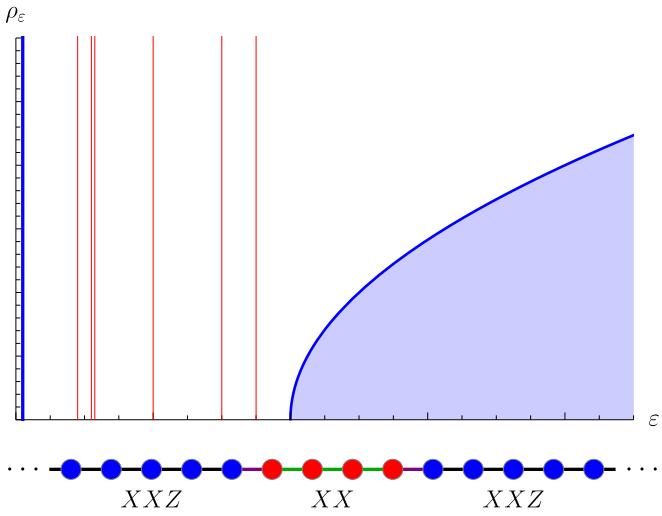

FIG. 1. (Bottom) A schematic of a finite-size XX spin-1/2 chain (red circles) sandwiched between two long anisotropic Heisenberg (XXZ) spin-1/2 chains (blue circles). (Top) Density of states ρ_ϵ with energy ϵ of the sandwich depicting discrete energy (bound) states (red lines) arising from XX spin chain in the excitation gap between ground and first excited states of the boundary XXZ spin chains.

a daunting task. On the other hand, numerical techniques to calculate the dynamics of such coupled system-reservoir models are mostly limited to relatively small sizes and timescales. In this paper, we critically investigate the role of interactions in thermalizing bound states by applying large-scale numerics using the time-evolving block decimation (TEBD) algorithm [20–22].

We mainly study quench dynamics in a quantum XX spin-1/2 chain coupled to two anisotropic Heisenberg (XXZ) spin-1/2 chains, one on either side (see Fig. 1), by following the time evolution of the full density matrix after the quench. The XXZ spin chains with an excitation energy gap between the ground and excited states act as boundary reservoirs with nontrivial (nonquadratic) interactions between spins. The quantum XX spin chain of short length (compared to the boundary wires) as the central system in the middle has a gapless continuous spectrum with spins that can be considered trivially (quadratic) interacting. We take very long lengths for both boundary chains in our numerics to avoid Poincaré recurrence and boundary effects (see Appendix A for details). We calculate the time evolution of magnetization and spin current in the entire system. We are specifically interested in detecting the relaxation dynamics of these quantities inside the middle XX chain. We observe thermalization of the central system with the interacting reservoirs even in the presence of bound states when the length M of the central system is relatively short ($M \leqslant 3$), which is sharply different from the case for the noninteracting reservoirs [19]. For a longer central system ($M > 3$), we find a strong signature of very slow (or absent) relaxation of some particular modes of the magnetization and spin current inside the XX spin chain. The frequencies of these special slow modes are related to the energies of states within the excitation gaps of the boundary XXZ chains that remain localized to the middle XX chain.

II. THE MODEL

The Hamiltonian of the coupled spin-1/2 chains can be written in a general form as

$$\mathcal{H} = -\sum_{l=1}^{N-1}\sum_{\alpha} J_l^\alpha \sigma_l^\alpha \sigma_{l+1}^\alpha, \tag{1}$$

where $\sigma_l^\alpha, \alpha \in \{x, y, z\}$ is the Pauli matrix at site l, and J_l^α is the exchange coupling between the α component of spins at sites l and $l+1$. The choice of exchange couplings defines the system, boundary reservoirs, and their interfaces. We choose the boundary chains of length L in the regions $l \in [1, L]$ and $l \in [L+M+1, N]$, and the middle chain of length M is at $l \in [L+1, L+M]$. We take the exchange couplings for the boundary chain as $J_l^x = J_l^y = J_l^z/\Delta = J_0$. The middle XX chain has $J_l^x = J_l^y = J_1$ and $J_l^z = 0$. The XX-type couplings at the interfaces are $J_l^x = J_l^y = J'$ and $J_l^z = 0$ for $l \in \{L, L+M\}$. The spin current operator is defined as $I_l = 2J_l(\sigma_l^y\sigma_{l+1}^x - \sigma_l^x\sigma_{l+1}^y)$, where J_l is the value of the hopping between sites l and $l+1$. The expectation value of the spin current is defined as $\langle I_l(t)\rangle = \mathrm{Tr}[\rho(t)I_l]$, where $\rho(t)$ is the density matrix of the full system at time t. We mostly investigate the quench dynamics of coupled spin chains in the XXZ-XX-XXZ configuration, where we choose $J_1/J_0 = 0.2$, $J'/J_0 = 0.05$, and $\Delta = 2$. The choice of parameters here is such that some energy states of the full system appear within the gap of the two boundary chains (which have a nonzero gap for $\Delta > 1$) due to the coupling to the XX chain. Additionally, we have also simulated the quench dynamics of coupled spin chains in the XXX-XX-XXX configuration for comparison, since the XXX boundary chains are gapless. In the latter case, we simply fix $\Delta = 1$, leaving the other parameters unchanged [23].

III. QUENCH PROTOCOLS AND RESULTS

In our numerical investigation of quench dynamics, we typically set the initial density matrix of the two boundary XXZ or XXX chains to a high-temperature state with constant magnetization in the z direction. For the middle XX chain, we choose a random magnetization profile (see Appendix A for details). In general the initial density matrix takes the product form

$$\rho(0) \propto \bigotimes_{l=1}^{N} e^{\mu_l \sigma_l^z}, \tag{2}$$

where the parameters μ_l determine the initial magnetization at each site. We choose μ_l to be small for all l, such that our state is effectively a high-temperature state. We then evolve the density matrix $\rho(t)$ of the full system from the initial density matrix $\rho(0)$ using $\rho(t) = e^{-i\mathcal{H}t/\hbar}\rho(0)e^{i\mathcal{H}t/\hbar}$, and we follow the time evolution of relevant local observables, such as the spin and spin current densities. We provide the details of the numerics using the TEBD algorithm in Appendix A.

In Fig. 2, we compare the relaxation dynamics of the XXX-XX-XXX and XXZ-XX-XXZ systems by looking at the time evolution of the spin current in the middle of the XX chain. It is immediately clear that in the case of XXX boundary chains the system quickly relaxes as the middle

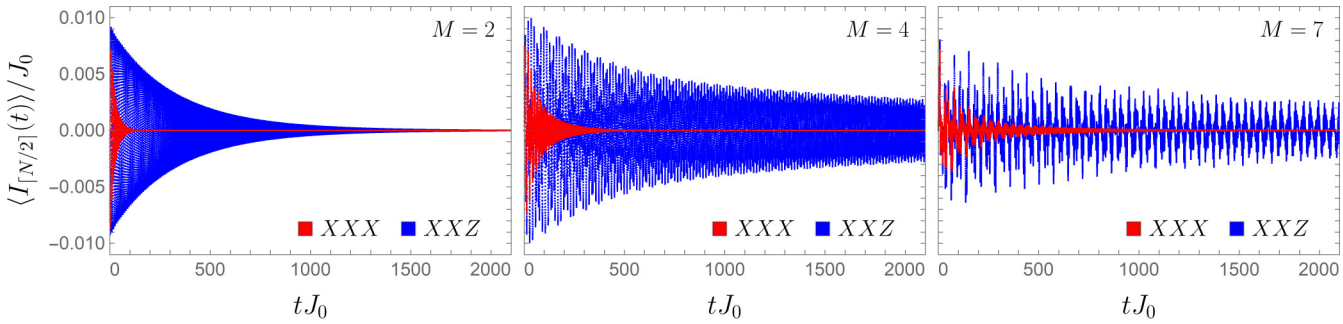

FIG. 2. Time evolution of spin current in the middle of the XX chain after the quench for both XXZ (blue) and XXX (red) boundary chains with various lengths of the middle segment. A clear difference in relaxation dynamics is observed since the system with gapped boundaries exhibits much slower (or no) decay in spin current oscillations compared to the gapless boundaries. In the initial state, the boundaries are at infinite temperature ($\mu = 0$) while the middle XX chain has a random magnetization profile (μ_l i.i.d. in $[-0.02, 0.02]$). We use $J_1/J_0 = 0.2$ and $J'/J_0 = 0.05$ in all cases, as well as $\Delta = 1$ for XXX and $\Delta = 2$ for XXZ. The length of the full system is set to $N = 720$ with the XX chain positioned in the middle.

chain thermalizes with the rest of the system. We note here that, even though the isolated XXX and XXZ chains are exactly solvable via Bethe ansatz, the coupled chains of XXX-XX-XXX or XXZ-XX-XXZ are not integrable [24]. Thus, the thermalization in XXX-XX-XXX is in line with the eigenstate thermalization hypothesis (ETH) [25]. On the other hand, looking at the system with XXZ boundary chains we notice clearly slower themalization or even lack thereof at larger M. Thus, the persistent oscillations of spin current in some particular frequency modes for larger M seem to suggest a violation of the ETH for XXZ-XX-XXZ systems. In Fig. 3, we further show the time dependence of the frequencies of these spin current oscillations in XXZ-XX-XXZ systems for different M. We observe that some frequencies are particularly stable and show (almost) no decay for greater M within the accessible times. We attribute this lack of thermalization in the XXZ case to the existence of states due to the middle chain that are within the gap of the boundary chains. To test this assertion, we now look at the eigenstate properties of shorter lengths of coupled chains, paying particular attention to eigenstates within the spectral gap of the boundary chains.

IV. EIGENSTATE PROPERTIES OF THE COUPLED CHAINS

In Fig. 4, we present a typical low-energy spectrum of an isolated ferromagnetic XXZ chain of length $N = 14$ and $\Delta/J_0 = 2$. It exhibits an excitation gap $\delta E_{\text{eg}}/J_0 = 3.0$ between two degenerate ground states ($\epsilon_1/J_0 = -26$) and the first excited states ($\epsilon_3/J_0 = -23$). In Fig. 4, we further show the energy eigenstates appearing within the excitation gap of isolated boundary chains in the low-energy spectrum of an XXZ-XX-XXZ system for $N = 14$, $L = 6$, and $M = 2$ and for $N = 14$, $L = 5$, and $M = 4$. Increasing the length of the full system by lengthening the leads only shifts the values of these energies but does not change the differences between the energies of the bound states and thus has no effect on our results (see Appendix A).

We notice that some of these mid-excitation-gap states have all spins pointing either up or down in both boundary chains and only have any nontrivial spin pattern in the middle chain. In the presence of some local perturbation, we can thus have local spin dynamics between these special states which is confined in the middle chain without affecting the

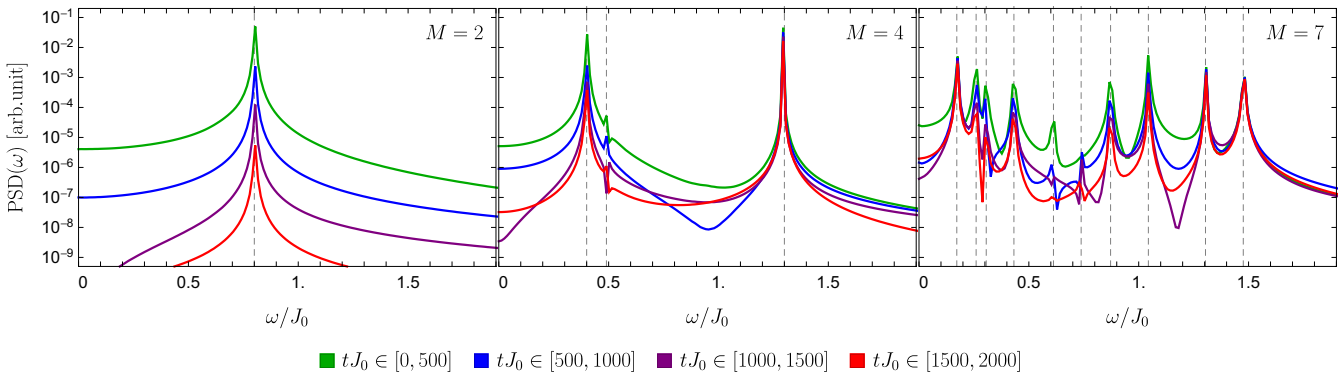

FIG. 3. Power spectral density (PSD) extracted from different time windows (solid colored lines) of the TEBD simulation for several sizes of M of the middle chain of XXZ-XX-XXZ. The gray dashed lines represent the frequencies of spin current oscillations obtained from bound state analysis using exact diagonalization on smaller systems. We can observe excellent agreement between the peaks in PSD and the computed frequencies. We see clear decay of the only existing frequency for $M = 2$. However, as we increase M, we begin to see modes with extremely slow or even no decay within the accuracy of our simulations. This suggests that these modes would not thermalize with the rest of the system and would maintain a memory of the initial conditions for long times.

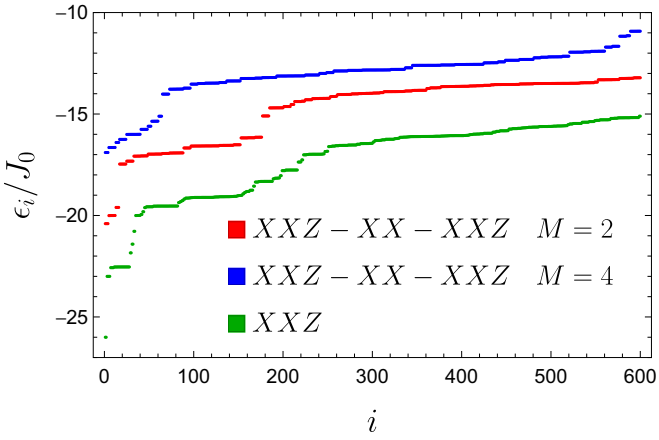

FIG. 4. Typical low-energy spectrum ϵ_i of an isolated XXZ spin-1/2 chain (green) with an excitation gap, and coupled spin-1/2 chains of the XXZ-XX-XXZ configuration (red and blue) with bound states within the excitation gap. The parameters are $J_1/J_0 = 0.2$, $J'/J_0 = 0.05$, and $\Delta = 2$ in all plots. The lengths are $L = N = 14$ (green); $N = 14$, $L = 6$, and $M = 2$ (red); and $N = 14$, $L = 5$, and $M = 4$ (blue).

boundary chains. Here we refer to these states as bound states, borrowing the notion from noninteracting models [16,19]. For example, we have such special bound states with energies $\epsilon_i/J_0 = -20.4$ and -19.6 for $N = 14$, $L = 6$, and $M = 2$:

$$|-20.4\rangle_\uparrow \approx |\uparrow\rangle_L \otimes (0.7068|\downarrow\uparrow\rangle + 0.7068|\uparrow\downarrow\rangle) \otimes |\uparrow\rangle_R,$$

$$|-19.6\rangle_\uparrow \approx |\uparrow\rangle_L \otimes (-0.7066|\downarrow\uparrow\rangle + 0.7066|\uparrow\downarrow\rangle) \otimes |\uparrow\rangle_R,$$

and $|-20.4\rangle_\downarrow$ and $|-19.6\rangle_\downarrow$ with all spins flipped compared to $|-20.4\rangle_\uparrow$ and $|-19.6\rangle_\uparrow$, respectively. Here the basis states $|\downarrow\rangle_{L/R}$ and $|\uparrow\rangle_{L/R}$ represent the state of left or right boundary chain with all spins $\downarrow$ and $\uparrow$, respectively. There are some other bound states of the form $|\uparrow\rangle_L \otimes |\uparrow\uparrow\rangle \otimes |\uparrow\rangle_R$, and $|\uparrow\rangle_L \otimes |\downarrow\downarrow\rangle \otimes |\uparrow\rangle_R$ as well as their spin-flipped partners at $\epsilon_i/J_0 = -20$, which we do not consider here since they do not affect the spin current dynamics in the middle of the XX chain that we are interested in. We emphasize that most eigenstates, including those with energy within the excitation gap of the XXZ-XX-XXZ system, are not of the above special forms and have nontrivial spin texture in both the middle and boundary chains. The bound states $|-20.4\rangle_{\uparrow,\downarrow}$ and $|-19.6\rangle_{\uparrow,\downarrow}$ still have some extremely small overlaps with the other basis states in their corresponding symmetry sectors. Thus, the spin orientations of the boundary chains are mostly the same for the states $|-20.4\rangle_{\uparrow,\downarrow}$ and $|-19.6\rangle_{\uparrow,\downarrow}$. A coherent oscillation of spin current at the middle of the XX chain occurs at an angular frequency of $0.8J_0$ ($\hbar = 1$) due to spin exchange between $|-20.4\rangle_{\uparrow,\downarrow}$ and $|-19.6\rangle_{\uparrow,\downarrow}$ upon application of the current operator. We find $\langle I_7(t)\rangle \propto \sin(0.8J_0 t)$. Nevertheless, the boundary chains directly connected to both of the spins in the middle act as a reservoir. Thus, the boundary chains would induce strong dephasing/decoherence to such coherent oscillation, and the oscillations will eventually die out even in the presence of a large excitation gap. While the coherent oscillation due to spin flip inside the middle chain should also decay due to the dephasing effect from the boundary chains for $M = 3$, it should survive for $M > 3$ where a coherent spin flip inside the middle chain between spins away from the interfaces is possible.

In order to observe such survival of oscillations, we extend the above analysis of bound states for an XXZ-XX-XXZ system of $N = 14$, $L = 5$, and $M = 4$. We find the energies of the bound states with a single spin flip in the XX chain for this case are $\epsilon_i/J_0 = -16.648$, -16.249, -15.755, and -15.354. We give the full expressions of the corresponding eigenstates in Appendix B, where we also discuss other multimagnon bound states and their contributions to spin current oscillations. The contribution of these single-magnon bound states to the expectation value of the spin current at the middle of the XX chain is found to be

$$\langle I_7(t)\rangle \propto [0.362c_0 \sin(1.29J_0 t) + 0.223c_1 \sin(0.4J_0 t) + 0.138c_2 \sin(0.49J_0 t) - 0.224c_3 \sin(0.4J_0 t)]. \tag{3}$$

Here the coefficients c_0, c_1, c_2, and c_3 depend on the initial state occupation amplitudes of these bound states and can be considered real for simplicity. The spin current in Eq. (3) oscillates in time at angular frequencies $1.29J_0$, $0.4J_0$, and $0.49J_0$. However, the amplitudes of these current oscillations essentially depend on the initialization (the coefficients c_0, c_1, c_2, and c_3) of these bound states. We further notice that the oscillation at the angular frequency $1.29J_0$ is arising from the bound states with energies -16.648 and -15.354, both of which have maximum amplitudes for spin flips of the middle spins (second and third spin for $M = 4$) away from the interface between the XX chain and the boundary chains (see Appendix B). Current oscillations at any other frequency do not have this feature. Therefore, considering faster dephasing of those bound states with higher amplitudes for spin flips near the interfaces, we predict that the coherent oscillation at the angular frequency $1.29J_0$ would survive for the longest time. We would like to emphasize here that for noninteracting reservoirs, the nonthermalization occurs even for shorter central systems (e.g., $M = 2$ and 3) and for all modes appearing from the bound states within the spectral gap (see, e.g., Ref. [19]). Therefore, the nontrivial many-body interactions in the boundary reservoirs significantly influence the physics of thermalization even in the presence of a spectral gap, and the simple picture for the inhomogeneous system as a conductor sandwiched between insulators is not apt here. We have further observed that the spin current oscillations can also appear due to bound states with multiple flipped spins in the middle XX chain. For example, we find the above angular frequencies $1.29J_0$, $0.4J_0$, and $0.49J_0$ can also emerge from the two-magnon bound states in Appendix B. We can easily extend the above analysis to longer middle XX chains.

In Fig. 3, we now compare the frequencies of spin current oscillations obtained from the above analysis with bound states to the frequencies found from TEBD simulations. The angular frequencies of current oscillations from TEBD match nicely with our predicted values from bound state analysis. Furthermore, we observe that our prediction on which modes will survive longest also holds; for instance, the oscillation at $\omega/J_0 \approx 1.29$ for $M = 4$ shows very little decay compared to oscillations at lower angular frequency. From this comparison, we can conclude that the extremely slow thermalization

or even the absence of thermalization indeed appears to be related to the bound states within the spectral gap of the boundary chains (acting as reservoirs), even in the presence of interactions within the boundary chains.

V. CONCLUSION

In this work, we have checked the necessary conditions for a good thermalizing reservoir by extending the analysis from earlier works with noninteracting reservoirs [16,19] to interacting ones. Using large-scale TEBD simulations, we showed that gapless interacting reservoirs appear to thermalize the system in question. On the other hand, interacting reservoirs with a spectral gap show prolonged thermalization, or even no thermalization for longer ($M > 3$) central systems [26]. This suggests the latter (e.g., superconductors and correlated magnets) are not ideal candidates for coupling to systems to study dissipative dynamics of longer central systems, e.g., as in Josephson junctions made of an insulating or metallic layer sandwiched between two gapped superconductors. Furthermore, we show that the frequencies of the persistent spin current oscillations we observed for XXZ boundary chains match nicely to the energy differences between the eigenstates that remain primarily localized within the middle chain and contribute to the spin current expectation value in the middle of the chain. We have also investigated the role of stronger couplings between XX and XXZ chains, suggesting an inevitable change in relaxation dynamics as the mid-excitation-gap states shift with increasing couplings. Our findings further indicate that an open quantum system description of transport depends not only on the properties of the system but also on those of the interfaces/couplings and reservoirs (e.g., spectral properties of reservoirs). Our study can be extended to understanding the relaxation dynamics of other correlated systems with various bound states, e.g., Yu-Shiba-Rusinov [27–29] and Majorana [30] bound states, which appear in the spectral gap of s-wave or p-wave superconductors. Another inhomogeneous many-body system of a magnetic impurity coupled to superconducting electrodes has been explored in Ref. [31], which appeared shortly after our study. It has been shown that the local Coulomb interactions do not provide an effective relaxation mechanism for the initially trapped quasiparticles in their study. Therefore, the emergence of nonthermalizing (slow) modes for gapped boundary spectrum even in the presence of interactions seems to be a general description for different inhomogeneous junctions. There is growing interest in understanding transport and nonequilibrium dynamics in inhomogeneous many-body quantum models by coupling multiple different systems [32], especially quantum spin chains [33,34], and our present results would be helpful in those studies with a spectral gap that mainly was unexplored.

ACKNOWLEDGMENTS

M.L. and T.P. acknowledge support from the European Research Council (ERC) through Grant No. 694544, OMNES, and Grant No. P1-0402 of the Slovenian Research Agency (ARRS). D.R. acknowledges support from the Ministry of Electronics & Information Technology (MeitY), India, under the grant for "Centre for Excellence in Quantum Technologies" (Grant No. 4(7)/2020-ITEA).

APPENDIX A: DETAILS ON NUMERICAL SIMULATIONS

Numerical simulations have been performed using two algorithms. For the time-evolution of spin current, we use the TEBD algorithm, which allows us to study very long system sizes. For the eigenstate properties, we apply exact diagonalization (ED) to obtain the eigenstates of the coupled chains at relatively short system sizes, as is typically the case with this method.

1. TEBD simulations

In TEBD simulations, we look at the time evolution of a density matrix which is initially prepared in a high-energy configuration:

$$\rho(t=0) = \left(\bigotimes_{i\in L} e^{\mu_L \sigma_i^z}\right) \otimes \left(\bigotimes_{i\in C} e^{\mu_{C,i} \sigma_i^z}\right) \otimes \left(\bigotimes_{i\in R} e^{\mu_R \sigma_i^z}\right), \tag{A1}$$

where L, C, and R represent the left, center, and right parts of the coupled spin-1/2 chains. We then choose $\mu_L = \mu_R = 0$, which can be interpreted as preparing the boundary chains at infinite temperature, and we select $\mu_{C,i}$ to be i.i.d. random variables in $[-0.1, 0.1]$ or $[-0.02, 0.02]$, which ensures some nontrivial distribution of initial magnetization in the central part. The density matrix is then evolved in time using TEBD. Here, we perform the time evolution with several bond dimensions ranging from very small $\chi = 32$ up to $\chi = 256$ (although the largest bond dimensions do not reach the required final times in reasonable simulation time). Comparing the results between these different bond dimensions, we determine whether the simulations are sufficiently converged. We note that while these bond dimensions are relatively small, these systems are unique since most entanglement is located in the central chain, which in turn is small and thus can be captured relatively well even with smaller bond dimensions.

The weak coupling to the boundary chains means that after an initial fast growth of entanglement in the middle, the growth slows down significantly, allowing us to reach the required final times with relatively good accuracy.

Several configurations are considered for the initial random magnetization in the central chain to ensure results are consistent, but only one configuration is run to these long times. The initial configuration only affects the weights corresponding to each eigenstate. Thus it merely affects the relative weights in the initial frequency spectrum of the spin current oscillations but does not change the decay rate (or lack thereof).

Finally, to ensure there is no finite-size effect in our simulations, we perform all simulations for two lengths of the entire system, $N = 360$ and $N = 720$, and compare the results to ensure they match to within numerical precision. We should note here that the nature of these dynamics is such that the spin expectation values become nonzero only for a much smaller part of the whole system, and even significantly smaller complete systems could be considered. Nevertheless,

the additional computational cost of sites in the boundary where bond dimension does not grow beyond 1 is negligible.

2. ED simulations

Exact diagonalization is performed for various symmetric configurations of the full system. At fixed M, we take several values of the length of the boundaries but always ensure they are symmetric to maintain reflection symmetry in the model. The diagonalization is then performed for all these cases and compared to ensure that the distances between the energy levels we are interested in are not affected by the finite size, as that would affect the corresponding frequencies. This is done by performing ED on the system of total length $N = 12$ up to $N = 21$. The actual diagonalization is done separately for each symmetry sector. We consider both magnetization and reflection symmetries of the entire system to minimize the sizes of these matrices and thus maximize the length we can study.

APPENDIX B: BOUND STATES FOR $M = 4$

In this section, we give explicit expressions of bound states with single or multiple flipped spins in the middle XX chain of an XXZ-XX-XXZ system of $N = 14$, $L = 5$, and $M = 4$. The single-magnon bound states with a single flipped spin in the middle XX chain are the following:

$$
\begin{aligned}
|-16.648\rangle_{\uparrow\uparrow} &\approx |\uparrow\rangle_L \otimes (0.372|\downarrow\uparrow\uparrow\uparrow\rangle + 0.601|\uparrow\downarrow\uparrow\uparrow\rangle + 0.601|\uparrow\uparrow\downarrow\uparrow\rangle + 0.372|\uparrow\uparrow\uparrow\downarrow\rangle) \otimes |\uparrow\rangle_R,\\
|-16.249\rangle_{\uparrow\uparrow} &\approx |\uparrow\rangle_L \otimes (-0.602|\downarrow\uparrow\uparrow\uparrow\rangle - 0.371|\uparrow\downarrow\uparrow\uparrow\rangle + 0.371|\uparrow\uparrow\downarrow\uparrow\rangle + 0.602|\uparrow\uparrow\uparrow\downarrow\rangle) \otimes |\uparrow\rangle_R,\\
|-15.755\rangle_{\uparrow\uparrow} &\approx |\uparrow\rangle_L \otimes (0.601|\downarrow\uparrow\uparrow\uparrow\rangle - 0.373|\uparrow\downarrow\uparrow\uparrow\rangle - 0.373|\uparrow\uparrow\downarrow\uparrow\rangle + 0.601|\uparrow\uparrow\uparrow\downarrow\rangle) \otimes |\uparrow\rangle_R,\\
|-15.354\rangle_{\uparrow\uparrow} &\approx |\uparrow\rangle_L \otimes (0.371|\downarrow\uparrow\uparrow\uparrow\rangle - 0.602|\uparrow\downarrow\uparrow\uparrow\rangle + 0.602|\uparrow\uparrow\downarrow\uparrow\rangle - 0.371|\uparrow\uparrow\uparrow\downarrow\rangle) \otimes |\uparrow\rangle_R,\\
|-16.648\rangle_{\downarrow\downarrow} &\approx |\downarrow\rangle_L \otimes (0.372|\uparrow\downarrow\downarrow\downarrow\rangle + 0.601|\downarrow\uparrow\downarrow\downarrow\rangle + 0.601|\downarrow\downarrow\uparrow\downarrow\rangle + 0.372|\downarrow\downarrow\downarrow\uparrow\rangle) \otimes |\downarrow\rangle_R,\\
|-16.249\rangle_{\downarrow\downarrow} &\approx |\downarrow\rangle_L \otimes (-0.602|\uparrow\downarrow\downarrow\downarrow\rangle - 0.371|\downarrow\uparrow\downarrow\downarrow\rangle + 0.371|\downarrow\downarrow\uparrow\downarrow\rangle + 0.602|\downarrow\downarrow\downarrow\uparrow\rangle) \otimes |\downarrow\rangle_R,\\
|-15.755\rangle_{\downarrow\downarrow} &\approx |\downarrow\rangle_L \otimes (0.601|\uparrow\downarrow\downarrow\downarrow\rangle - 0.373|\downarrow\uparrow\downarrow\downarrow\rangle - 0.373|\downarrow\downarrow\uparrow\downarrow\rangle + 0.601|\downarrow\downarrow\downarrow\uparrow\rangle) \otimes |\downarrow\rangle_R,\\
|-15.354\rangle_{\downarrow\downarrow} &\approx |\downarrow\rangle_L \otimes (0.371|\uparrow\downarrow\downarrow\downarrow\rangle - 0.602|\downarrow\uparrow\downarrow\downarrow\rangle + 0.602|\downarrow\downarrow\uparrow\downarrow\rangle - 0.371|\downarrow\downarrow\downarrow\uparrow\rangle) \otimes |\downarrow\rangle_R.
\end{aligned}
$$

The states are labeled by their energy and the magnetization of the left and right leads. Again, the bound states $|-16.648\rangle_{\uparrow\uparrow,\downarrow\downarrow}$, $|-16.249\rangle_{\uparrow\uparrow,\downarrow\downarrow}$, $|-15.755\rangle_{\uparrow\uparrow,\downarrow\downarrow}$, and $|-15.354\rangle_{\uparrow\uparrow,\downarrow\downarrow}$ have very small amplitudes to those basis states where one spin of the left or right boundary chain is flipped. As we have discussed in the main text, the persistent spin current oscillations can also result due to those bound states with multiple flipped spins in the middle XX chain. Below we provide two-magnon bound states with two flipped spins in the middle XX chain (as well as in the entire system), which also give rise to persistent spin current oscillations:

$$
\begin{aligned}
|-16.891\rangle_{\uparrow\uparrow} &\approx |\uparrow\rangle_L \otimes (0.224|\uparrow\uparrow\downarrow\downarrow\rangle + 0.224|\downarrow\downarrow\uparrow\uparrow\rangle + 0.5|\uparrow\downarrow\uparrow\downarrow\rangle + 0.5|\downarrow\uparrow\downarrow\uparrow\rangle + 0.446|\uparrow\downarrow\downarrow\uparrow\rangle + 0.448|\downarrow\uparrow\uparrow\downarrow\rangle) \otimes |\uparrow\rangle_R,\\
|-16.403\rangle_{\uparrow\uparrow} &\approx |\uparrow\rangle_L \otimes (0.5|\uparrow\uparrow\downarrow\downarrow\rangle - 0.5|\downarrow\downarrow\uparrow\uparrow\rangle + 0.5|\uparrow\downarrow\uparrow\downarrow\rangle - 0.5|\downarrow\uparrow\downarrow\uparrow\rangle) \otimes |\uparrow\rangle_R,\\
|-16.002\rangle_{\uparrow\uparrow} &\approx |\uparrow\rangle_L \otimes (-0.447|\uparrow\uparrow\downarrow\downarrow\rangle - 0.447|\downarrow\downarrow\uparrow\uparrow\rangle + 0.002|\uparrow\downarrow\uparrow\downarrow\rangle + 0.002|\downarrow\uparrow\downarrow\uparrow\rangle + 0.724|\uparrow\downarrow\downarrow\uparrow\rangle\\
&\quad - 0.276|\downarrow\uparrow\uparrow\downarrow\rangle) \otimes |\uparrow\rangle_R,\\
|-15.603\rangle_{\uparrow\uparrow} &\approx |\uparrow\rangle_L \otimes (0.5|\uparrow\uparrow\downarrow\downarrow\rangle - 0.5|\downarrow\downarrow\uparrow\uparrow\rangle - 0.5|\uparrow\downarrow\uparrow\downarrow\rangle + 0.5|\downarrow\uparrow\downarrow\uparrow\rangle) \otimes |\uparrow\rangle_R,\\
|-16.891\rangle_{\downarrow\downarrow} &\approx |\downarrow\rangle_L \otimes (0.224|\downarrow\downarrow\uparrow\uparrow\rangle + 0.224|\uparrow\uparrow\downarrow\downarrow\rangle + 0.5|\downarrow\uparrow\downarrow\uparrow\rangle + 0.5|\uparrow\downarrow\uparrow\downarrow\rangle + 0.446|\downarrow\uparrow\uparrow\downarrow\rangle + 0.448|\uparrow\downarrow\downarrow\uparrow\rangle) \otimes |\downarrow\rangle_R,\\
|-16.403\rangle_{\downarrow\downarrow} &\approx |\downarrow\rangle_L \otimes (0.5|\downarrow\downarrow\uparrow\uparrow\rangle - 0.5|\uparrow\uparrow\downarrow\downarrow\rangle + 0.5|\downarrow\uparrow\downarrow\uparrow\rangle - 0.5|\uparrow\downarrow\uparrow\downarrow\rangle) \otimes |\downarrow\rangle_R,\\
|-16.002\rangle_{\downarrow\downarrow} &\approx |\downarrow\rangle_L \otimes (-0.447|\downarrow\downarrow\uparrow\uparrow\rangle - 0.447|\uparrow\uparrow\downarrow\downarrow\rangle + 0.002|\downarrow\uparrow\downarrow\uparrow\rangle + 0.002|\uparrow\downarrow\uparrow\downarrow\rangle + 0.724|\downarrow\uparrow\uparrow\downarrow\rangle\\
&\quad - 0.276|\uparrow\downarrow\downarrow\uparrow\rangle) \otimes |\downarrow\rangle_R,\\
|-15.603\rangle_{\downarrow\downarrow} &\approx |\downarrow\rangle_L \otimes (0.5|\downarrow\downarrow\uparrow\uparrow\rangle - 0.5|\uparrow\uparrow\downarrow\downarrow\rangle - 0.5|\downarrow\uparrow\downarrow\uparrow\rangle + 0.5|\uparrow\downarrow\uparrow\downarrow\rangle) \otimes |\downarrow\rangle_R.
\end{aligned}
$$

These two-magnon bound states contribute to spin current oscillations at angular frequencies $1.29J_0$, $0.49J_0$, and $0.4J_0$, which can be determined by taking the expectation of the spin current operator in these states. There are no nontrivial bound states in the three-magnon, four-magnon, and five-magnon sectors which can contribute to spin current oscillations. The bound states in

the six-magnon sector contribute to spin current oscillation at frequency $0.4J_0$:

$$
\begin{aligned}
|-16.650\rangle_{\uparrow\downarrow} &\approx |\uparrow\rangle_L \otimes (0.370|\uparrow\uparrow\uparrow\downarrow\rangle + 0.600|\uparrow\uparrow\downarrow\uparrow\rangle + 0.602|\uparrow\downarrow\uparrow\uparrow\rangle + 0.364|\downarrow\uparrow\uparrow\uparrow\rangle) \otimes |\downarrow\rangle_R,\\
|-16.250\rangle_{\uparrow\downarrow} &\approx |\uparrow\rangle_L \otimes (0.600|\uparrow\uparrow\uparrow\downarrow\rangle + 0.375|\uparrow\uparrow\downarrow\uparrow\rangle - 0.370|\uparrow\downarrow\uparrow\uparrow\rangle - 0.602|\downarrow\uparrow\uparrow\uparrow\rangle) \otimes |\downarrow\rangle_R,\\
|-16.650\rangle_{\downarrow\uparrow} &\approx |\downarrow\rangle_L \otimes (0.370|\downarrow\uparrow\uparrow\uparrow\rangle + 0.600|\uparrow\downarrow\uparrow\uparrow\rangle + 0.602|\uparrow\uparrow\downarrow\uparrow\rangle + 0.364|\uparrow\uparrow\uparrow\downarrow\rangle) \otimes |\uparrow\rangle_R,\\
|-16.250\rangle_{\downarrow\uparrow} &\approx |\downarrow\rangle_L \otimes (0.600|\downarrow\uparrow\uparrow\uparrow\rangle + 0.375|\uparrow\downarrow\uparrow\uparrow\rangle - 0.370|\uparrow\uparrow\downarrow\uparrow\rangle - 0.602|\uparrow\uparrow\uparrow\downarrow\rangle) \otimes |\uparrow\rangle_R,\\
|-16.650\rangle_{\downarrow\uparrow} &\approx |\downarrow\rangle_L \otimes (0.370|\downarrow\downarrow\downarrow\uparrow\rangle + 0.600|\downarrow\downarrow\uparrow\downarrow\rangle + 0.602|\downarrow\uparrow\downarrow\downarrow\rangle + 0.364|\uparrow\downarrow\downarrow\downarrow\rangle) \otimes |\uparrow\rangle_R,\\
|-16.250\rangle_{\downarrow\uparrow} &\approx |\downarrow\rangle_L \otimes (0.600|\downarrow\downarrow\downarrow\uparrow\rangle + 0.375|\downarrow\downarrow\uparrow\downarrow\rangle - 0.370|\downarrow\uparrow\downarrow\downarrow\rangle - 0.602|\uparrow\downarrow\downarrow\downarrow\rangle) \otimes |\uparrow\rangle_R,\\
|-16.650\rangle_{\uparrow\downarrow} &\approx |\uparrow\rangle_L \otimes (0.370|\uparrow\downarrow\downarrow\downarrow\rangle + 0.600|\downarrow\uparrow\downarrow\downarrow\rangle + 0.602|\downarrow\downarrow\uparrow\downarrow\rangle + 0.364|\downarrow\downarrow\downarrow\uparrow\rangle) \otimes |\downarrow\rangle_R,\\
|-16.250\rangle_{\uparrow\downarrow} &\approx |\uparrow\rangle_L \otimes (0.600|\uparrow\downarrow\downarrow\downarrow\rangle + 0.375|\downarrow\uparrow\downarrow\downarrow\rangle - 0.370|\downarrow\downarrow\uparrow\downarrow\rangle - 0.602|\downarrow\downarrow\downarrow\uparrow\rangle) \otimes |\downarrow\rangle_R.
\end{aligned}
$$

Finally, there are nontrivial bound states in the seven-magnon sector (or the zero magnetization of the full system), which can also contribute in spin current oscillations at angular frequencies $1.29J_0$, $0.49J_0$, and $0.4J_0$. These bound states are represented with fixed magnetization on the left and right sides for compactness, and hence they lack reflection symmetry/asymmetry with respect to the middle of the full system. These states are written as linear combinations of exactly degenerate (within numerical accuracy) states from the symmetric/antisymmetric sectors:

$$
\begin{aligned}
|-16.897\rangle_{\downarrow\uparrow} \approx{}& |\downarrow\rangle_L \otimes (-0.225|\uparrow\uparrow\downarrow\downarrow\rangle - 0.502|\uparrow\downarrow\uparrow\downarrow\rangle - 0.447|\uparrow\downarrow\downarrow\uparrow\rangle - 0.447|\downarrow\uparrow\uparrow\downarrow\rangle - 0.498|\downarrow\uparrow\downarrow\uparrow\rangle\\
&- 0.222|\downarrow\downarrow\uparrow\uparrow\rangle) \otimes |\uparrow\rangle_R,\\
|-16.403\rangle_{\downarrow\uparrow} \approx{}& |\downarrow\rangle_L \otimes (-0.501|\uparrow\uparrow\downarrow\downarrow\rangle - 0.498|\uparrow\downarrow\uparrow\downarrow\rangle + 0.502|\downarrow\uparrow\downarrow\uparrow\rangle + 0.498|\downarrow\downarrow\uparrow\uparrow\rangle) \otimes |\uparrow\rangle_R,\\
|-16.003\rangle_{\downarrow\uparrow} \approx{}& |\downarrow\rangle_L \otimes (0.632|\uparrow\uparrow\downarrow\downarrow\rangle - 0.316|\uparrow\downarrow\downarrow\uparrow\rangle - 0.316|\downarrow\uparrow\uparrow\downarrow\rangle + 0.632|\downarrow\downarrow\uparrow\uparrow\rangle) \otimes |\uparrow\rangle_R,\\
|-16.003\rangle_{\downarrow\uparrow} \approx{}& |\downarrow\rangle_L \otimes (0.707|\uparrow\downarrow\downarrow\uparrow\rangle - 0.707|\downarrow\uparrow\uparrow\downarrow\rangle) \otimes |\uparrow\rangle_R,\\
|-15.603\rangle_{\downarrow\uparrow} \approx{}& |\downarrow\rangle_L \otimes (-0.498|\uparrow\uparrow\downarrow\downarrow\rangle + 0.501|\uparrow\downarrow\uparrow\downarrow\rangle - 0.498|\downarrow\uparrow\downarrow\uparrow\rangle + 0.502|\downarrow\downarrow\uparrow\uparrow\rangle) \otimes |\uparrow\rangle_R,\\
|-15.109\rangle_{\downarrow\uparrow} \approx{}& |\downarrow\rangle_L \otimes (-0.222|\uparrow\uparrow\downarrow\downarrow\rangle + 0.497|\uparrow\downarrow\uparrow\downarrow\rangle - 0.447|\uparrow\downarrow\downarrow\uparrow\rangle - 0.447|\downarrow\uparrow\uparrow\downarrow\rangle + 0.502|\downarrow\uparrow\downarrow\uparrow\rangle\\
&- 0.225|\downarrow\downarrow\uparrow\uparrow\rangle) \otimes |\uparrow\rangle_R,\\
|-16.897\rangle_{\uparrow\downarrow} \approx{}& |\uparrow\rangle_L \otimes (-0.225|\downarrow\downarrow\uparrow\uparrow\rangle - 0.502|\downarrow\uparrow\downarrow\uparrow\rangle - 0.447|\downarrow\uparrow\uparrow\downarrow\rangle - 0.447|\uparrow\downarrow\downarrow\uparrow\rangle - 0.498|\uparrow\downarrow\uparrow\downarrow\rangle\\
&- 0.222|\uparrow\uparrow\downarrow\downarrow\rangle) \otimes |\downarrow\rangle_R,\\
|-16.403\rangle_{\uparrow\downarrow} \approx{}& |\uparrow\rangle_L \otimes (-0.501|\downarrow\downarrow\uparrow\uparrow\rangle - 0.498|\downarrow\uparrow\downarrow\uparrow\rangle + 0.502|\uparrow\downarrow\uparrow\downarrow\rangle + 0.498|\uparrow\uparrow\downarrow\downarrow\rangle) \otimes |\downarrow\rangle_R,\\
|-16.003\rangle_{\uparrow\downarrow} \approx{}& |\uparrow\rangle_L \otimes (0.632|\downarrow\downarrow\uparrow\uparrow\rangle - 0.316|\downarrow\uparrow\uparrow\downarrow\rangle - 0.316|\uparrow\downarrow\downarrow\uparrow\rangle + 0.632|\uparrow\uparrow\downarrow\downarrow\rangle) \otimes |\downarrow\rangle_R,\\
|-16.003\rangle_{\uparrow\downarrow} \approx{}& |\uparrow\rangle_L \otimes (0.707|\downarrow\uparrow\uparrow\downarrow\rangle - 0.707|\uparrow\downarrow\downarrow\uparrow\rangle) \otimes |\downarrow\rangle_R,\\
|-15.603\rangle_{\uparrow\downarrow} \approx{}& |\uparrow\rangle_L \otimes (-0.498|\downarrow\downarrow\uparrow\uparrow\rangle + 0.501|\downarrow\uparrow\downarrow\uparrow\rangle - 0.498|\uparrow\downarrow\uparrow\downarrow\rangle + 0.502|\uparrow\uparrow\downarrow\downarrow\rangle) \otimes |\downarrow\rangle_R,\\
|-15.109\rangle_{\uparrow\downarrow} \approx{}& |\uparrow\rangle_L \otimes (-0.222|\downarrow\downarrow\uparrow\uparrow\rangle + 0.497|\downarrow\uparrow\downarrow\uparrow\rangle - 0.447|\downarrow\uparrow\uparrow\downarrow\rangle - 0.447|\uparrow\downarrow\downarrow\uparrow\rangle + 0.502|\uparrow\downarrow\uparrow\downarrow\rangle\\
&- 0.225|\uparrow\uparrow\downarrow\downarrow\rangle) \otimes |\downarrow\rangle_R.
\end{aligned}
$$

[1] G. Benenti, G. Casati, K. Saito, and R. S. Whitney, Fundamental aspects of steady-state conversion of heat to work at the nanoscale, Phys. Rep. **694**, 1 (2017).

[2] G. T. Landi, D. Poletti, and G. Schaller, Non-equilibrium boundary driven quantum systems: models, methods and properties, arXiv:2104.14350 [quant-ph].

[3] B. Bertini, F. Heidrich-Meisner, C. Karrasch, T. Prosen, R. Steinigeweg, and M. Žnidarič, Finite-temperature transport in one-dimensional quantum lattice models, Rev. Mod. Phys. **93**, 025003 (2021).

[4] R. Landauer, Spatial variation of currents and fields due to localized scatterers in metallic conduction, IBM J. Res. Dev. **1**, 223 (1957).

[5] R. Landauer, Electrical resistance of disordered one-dimensional lattices, Philos. Mag. **21**, 863 (1970).

[6] M. Büttiker, Four-Terminal Phase-Coherent Conductance, Phys. Rev. Lett. **57**, 1761 (1986).

[7] S. Kohler, J. Lehmann, and P. Hänggi, Driven quantum transport on the nanoscale, Phys. Rep. **406**, 379 (2005).

[8] Y. V. Nazarov and Y. M. Blanter, *Quantum Transport: Introduction to Nanoscience* (Cambridge University Press, Cambridge, England, 2009).

[9] R. de Picciotto, H. L. Stormer, L. N. Pfeiffer, K. W. Baldwin, and K. W. West, Four-terminal resistance of a ballistic quantum wire, Nature (London) **411**, 51 (2001).

[10] U. Weiss, *Quantum Dissipative Systems*, 4th ed. (World Scientific, Singapore, 2012).

[11] A. Dhar and B. S. Shastry, Quantum transport using the Ford-Kac-Mazur formalism, Phys. Rev. B **67**, 195405 (2003).
[12] D. Segal, A. Nitzan, and P. Hänggi, Thermal conductance through molecular wires, J. Chem. Phys. **119**, 6840 (2003).
[13] A. Dhar and D. Roy, Heat transport in harmonic lattices, J. Stat. Phys. **125**, 801 (2006).
[14] D. Karevski and T. Platini, Quantum Nonequilibrium Steady States Induced by Repeated Interactions, Phys. Rev. Lett. **102**, 207207 (2009).
[15] L. Arrachea, G. S. Lozano, and A. A. Aligia, Thermal transport in one-dimensional spin heterostructures, Phys. Rev. B **80**, 014425 (2009).
[16] A. Dhar and D. Sen, Nonequilibrium Green's function formalism and the problem of bound states, Phys. Rev. B **73**, 085119 (2006).
[17] M. Zgirski, L. Bretheau, Q. Le Masne, H. Pothier, D. Esteve, and C. Urbina, Evidence for Long-Lived Quasiparticles Trapped in Superconducting Point Contacts, Phys. Rev. Lett. **106**, 257003 (2011).
[18] R. S. Souto, A. Martín-Rodero, and A. L. Yeyati, Andreev Bound States Formation and Quasiparticle Trapping in Quench Dynamics Revealed by Time-Dependent Counting Statistics, Phys. Rev. Lett. **117**, 267701 (2016).
[19] N. Bondyopadhaya and D. Roy, Dynamics of hybrid junctions of Majorana wires, Phys. Rev. B **99**, 214514 (2019).
[20] G. Vidal, Efficient Classical Simulation of Slightly Entangled Quantum Computations, Phys. Rev. Lett. **91**, 147902 (2003).
[21] G. Vidal, Efficient Simulation of One-Dimensional Quantum Many-Body Systems, Phys. Rev. Lett. **93**, 040502 (2004).
[22] U. Schollwöck, The density-matrix renormalization group in the age of matrix product states, Ann. Phys. (NY) **326**, 96 (2011).
[23] Since we discuss here the relaxation dynamics of the middle chain to the effective high-temperature state of the boundary chains, we believe our main conclusions are independent of special low-energy features at $\Delta = 1$ in comparison to $\Delta < 1$ [35] as long as the boundary wires are gapless.
[24] M. Brenes, E. Mascarenhas, M. Rigol, and J. Goold, High-temperature coherent transport in the XXZ chain in the presence of an impurity, Phys. Rev. B **98**, 235128 (2018).
[25] J. M. Deutsch, Eigenstate thermalization hypothesis, Rep. Prog. Phys. **81**, 082001 (2018).
[26] J. Mossel and J.-S. Caux, Relaxation dynamics in the gapped XXZ spin-1/2 chain, New J. Phys. **12**, 055028 (2010).
[27] Yu Luh, Bound state in superconductors with paramagnetic impurities, Acta Phys. Sin. **21**, 75 (1965).
[28] H. Shiba, Classical spins in superconductors, Prog. Theor. Phys. **40**, 435 (1968).
[29] A. I. Rusinov, Superconductivity near a paramagnetic impurity, Zh. Eksp. Teor. Fiz. **9**, 146 (1969) [Sov. JETP Lett. **9**, 85 (1969)].
[30] E. Majorana, A symmetric theory of electrons and positrons, Nuovo Cimento **14**, 171 (1937).
[31] R. Seoane Souto, A. E. Feiguin, A. Martín-Rodero, and A. L. Yeyati, Transient dynamics of a magnetic impurity coupled to superconducting electrodes: Exact numerics versus perturbation theory, Phys. Rev. B **104**, 214506 (2021).
[32] R. Vasseur, J. P. Dahlhaus, and J. E. Moore, Universal Nonequilibrium Signatures of Majorana Zero Modes in Quench Dynamics, Phys. Rev. X **4**, 041007 (2014).
[33] A. Biella, M. Collura, D. Rossini, A. De Luca, and L. Mazza, Ballistic transport and boundary resistances in inhomogeneous quantum spin chains, Nat. Commun. **10**, 4820 (2019).
[34] G. Del Vecchio Del Vecchio, A. De Luca, and A. Bastianello, Transport through interacting defects and lack of thermalisation, SciPost Phys. **12**, 060 (2022).
[35] C. Karrasch and J. E. Moore, Luttinger liquid physics from the infinite-system density matrix renormalization group, Phys. Rev. B **86**, 155156 (2012).